

# Analysis and Optimization of InGaAsP Electro-Absorption Modulators

D. Meglio, P. Lugli, R. Sabella, *Member, IEEE*, and O. Sahlén

**Abstract**—A numerical model of bulk electro-absorption modulators has been developed based on a quasi-two-dimensional drift-diffusion approach which includes both the presence of hetero-structures and the Fermi statistics for the carriers. We show that the nonlinear behavior of this type of devices is essentially related to hole pile-up and space-charge effects. The simulation results compare favourably with some laboratory measurements on a fabricated device with abrupt hetero-junctions. Two other types of structures have been simulated, one obtained with the inclusion of a thin quaternary layer and the other with a graded hetero-junction, which eliminate the hole pile-up at the InGaAsP-InP hetero-interface. The paper demonstrates that it is possible to approach the optimum behavior using both the alternatives considered here. Finally, nonlinear effects in short modulators have been investigated.

## I. INTRODUCTION

THE direct current modulation of single-longitudinal mode semiconductor lasers causes a dynamic variation of the peak emission wavelength, especially at high bit rates. The intermingling of such linewidth broadening (chirping) with the chromatic dispersion characteristics of single-mode optical fibres causes signal distortion and, eventually, generates intersymbol interference with consequent transmission penalties. As a result the bit-rate and span product is reduced. Therefore, in order to achieve multiple gigabit transmission over large distances, the use of low-chirp light sources is necessary.

An applicable approach is to use an external modulator that allows the laser to work in CW. Among several candidates (see [1]) the bulk electro-absorption modulator represents a promising solution. It can, indeed, operate at high speed, presents low chirp and is particularly suitable for monolithic integration with a single-mode laser. Furthermore it requires low driving voltages.

Unfortunately a degradation of the extinction ratio occurs when the optical input power increases (see the experiments reported in [2]). Two main causes are accountable for this effect: the hole pile-up and the space-charge effect. The former is due to the large number of photogenerated holes trapped at the valence band discontinuity of the p-InP-i-InGaAsP hetero-interface (see the scheme in Fig. 1) in the depletion region. The accumulation of trapped holes induces a large potential

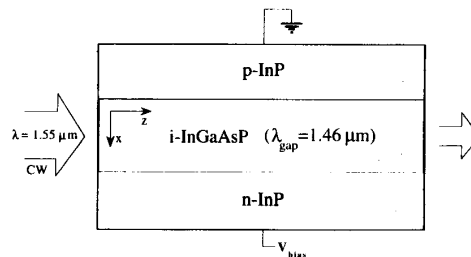


Fig. 1. Basic scheme of the modulator waveguide.

drop at the hetero-interface, thus reducing the electric field (and therefore the total electro-absorption) of the other region. Hence, the waveguide becomes more transparent. The latter effect is due to the large amount of space charge generated in the waveguide by electro-absorption of high input optical power, which instantly produces an internal electric field which tends to screen out the applied bias.

An alternative approach to bulk electro-absorption modulators is to use multiple-quantum well (MQW) modulators. These could be either of the Quantum-Confined Stark Effect (QCSE) type or of the Wannier-Stark (WS) type. Generally speaking, MQW modulators offer lower driving voltages for a specified extinction ratio. However, the saturation effects can be larger in MQW modulators than in bulk devices, due to the larger number of hetero-interfaces. Furthermore, the wavelength dependence when operating close to the exciton resonance can be larger than in bulk devices. High-speed, low-chirp MQW-modulators of both the QCSE type [3] and the WS type [4] have been reported.

In order to reduce the hole pile-up at the hetero-junction, the insertion of a quaternary buffer layer (InGaAsP) whose bandgap-wavelength is intermediate between those of the InP layer and InGaAsP absorbing layer has been proposed in [2]. Another approach, that we also consider in this paper, is the achievement of graded band-gap structures.

In the present paper we report, for the first time, a complete analysis on such issues. In particular, we have developed a quasi-two-dimensional numerical model, based on drift-diffusion approach that also includes the hetero-structure models and the Fermi statistics for the carriers, which allows us to analyse the static characteristics of this kind of modulator for any type of structure, aiming at the optimization of the device. In the present paper we investigate and compare the performance of three different device structures: the abrupt junction (AJ), the graded bandgap (GB) and the quaternary

Manuscript received April 25, 1994; revised August 29, 1994.

D. Meglio and P. Lugli are with the Università "Tor Vergata", Dipartimento di Elettronica, Rome, Italy.

R. Sabella is with Ericsson Telecomunicazioni, R & D Division, Rome, Italy.

O. Sahlén is with Ericsson Components, Fiber Optics Research Centre, Stockholm, Sweden.

IEEE Log Number 9407798.

(InGaAsP) inserted (QI) layer. The paper is organized as follows. In Section II and III, we describe the numerical model and the solution algorithm, respectively. The simulation results for a Franz–Keldysh modulator have been compared with the experimental ones in Section IV. Such experiments have been accomplished on a device similar to that reported in [5]. Then, in Section V, we discuss the alternative structures that allow to reduce the nonlinear effects while, in Section VI, we estimate the influence of the device length on the device performance.

## II. THE MATHEMATICAL MODEL

The modulator waveguide scheme is shown in Fig. 1. The quasi-two-dimensional model adopted here is based on a self-consistent solution of the coupled Poisson, continuity and transport equations along the  $x$ -direction:

*Poisson's equation*

$$\frac{d}{dx} \left( \varepsilon \frac{d\Psi}{dx} \right) = -q(p - n + N_D - N_A) \quad (1)$$

*continuity equation for electrons*

$$\frac{1}{q} \frac{dJ_n}{dx} + G - R = 0 \quad (2)$$

*continuity equation for holes*

$$-\frac{1}{q} \frac{dJ_p}{dx} + G - R = 0 \quad (3)$$

where  $\Psi$  denotes the electrostatic potential,  $p$  and  $n$ , respectively, the hole and electron concentrations,  $q$  is the electron charge magnitude,  $\varepsilon$  is the dielectric constant,  $N_A$  and  $N_D$  are the acceptor and donor impurity concentrations, respectively,  $G$  depicts the carrier radiative generation term and  $R$  is the Shockley–Read–Hall net recombination rate (the Auger recombination can be omitted because the carrier concentrations are not sufficiently high). The carrier transport in inhomogeneous media including hetero-structures can be originally described by the Boltzmann transport equation and the current is given by the gradient of the quasi-Fermi level. The electron/hole current densities in (2) and (3) can be written as

$$J_n = -q \cdot \mu_n(E) \cdot n \cdot \frac{d\varphi_n}{dx} \quad (4)$$

$$J_p = -q \cdot \mu_p(E) \cdot p \cdot \frac{d\varphi_p}{dx}. \quad (5)$$

Here,  $\varphi_n$  and  $\varphi_p$  are the electron and hole quasi-Fermi potentials, while  $\mu_n(E)$  and  $\mu_p(E)$  denote the carrier mobilities for electrons and holes, respectively, determined from the carrier velocities which are reported in [6], [7] as functions of the electric field. We are considering only thermoionic contribution to the current through the hetero-layers. Tunneling contributions are neglected since our calculations based on WKB approximation for triangular barriers have shown that they are, indeed, negligible.

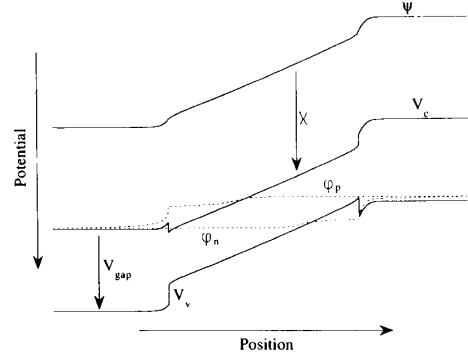


Fig. 2. Schematic band diagram of p-i-n hetero-structure.

Carrier degeneracy is considered defining the electron and hole densities as

$$n = N_C \cdot F_{1/2} \left( \frac{V_C - \varphi_n}{V_T} \right) \quad (6)$$

$$p = N_V \cdot F_{1/2} \left( \frac{\varphi_p - V_V}{V_T} \right) \quad (7)$$

where  $N_C$  and  $N_V$  are the effective densities of states in conduction and valence bands,  $V_C$  and  $V_V$  are the potentials of conduction and valence band edges,  $V_T$  is the thermal voltage, and  $F_{1/2}$  is the Fermi–Dirac integral of order 1/2 defined as

$$F_{1/2}(x) = \frac{2}{\sqrt{\pi}} \cdot \int_0^{\infty} \frac{\sqrt{y}}{1 + e^{y-x}} dy. \quad (8)$$

The relation between  $\varphi_p$ ,  $\varphi_n$ ,  $\Psi$ , the electron affinity  $\chi$ , and the potential gap  $V_{\text{gap}}$  is schematically depicted in Fig. 2. All material parameters are supposed to vary with position, according to the As percentage in the quaternary layer [6]–[9].

Since the light intensity decreases as it propagates along the  $z$  direction, according to the absorption, the device is therefore divided in longitudinal sections, each of length  $\Delta z$ . If  $L$  is the length of the device, there are  $L/\Delta z$  sections. The above equations are solved for each section, and the output from one section is used as input to the subsequent section. In each longitudinal section, the generation term is evaluated as:

$$G(x, z) = \frac{\alpha(E)}{h\nu} I(x, z) \quad (9)$$

where the intensity profile  $I(x, z)$  at  $z$  is calculated assuming fundamental mode propagation [10], and  $h\nu$  is the photon energy. The absorption coefficient  $\alpha$  as a function of the electric field has been treated in [11]–[13].

It is to be noticed that in a truly two-dimensional model the semiconductor equations and the Poisson's equation would directly contain the propagation direction so as to account for the gradient of the carrier concentration along this direction; while our model is a quasi-two-dimensional analytical representation of the device and, consequently, carrier motion in  $z$ -direction is neglected. Nevertheless we have verified that, indeed, the diffusion current along the  $z$ -direction is negligible.

The boundary conditions, needed for the system solutions, are determined by imposing thermal equilibrium in the semiconductor at the border of the quasi-neutral regions of the

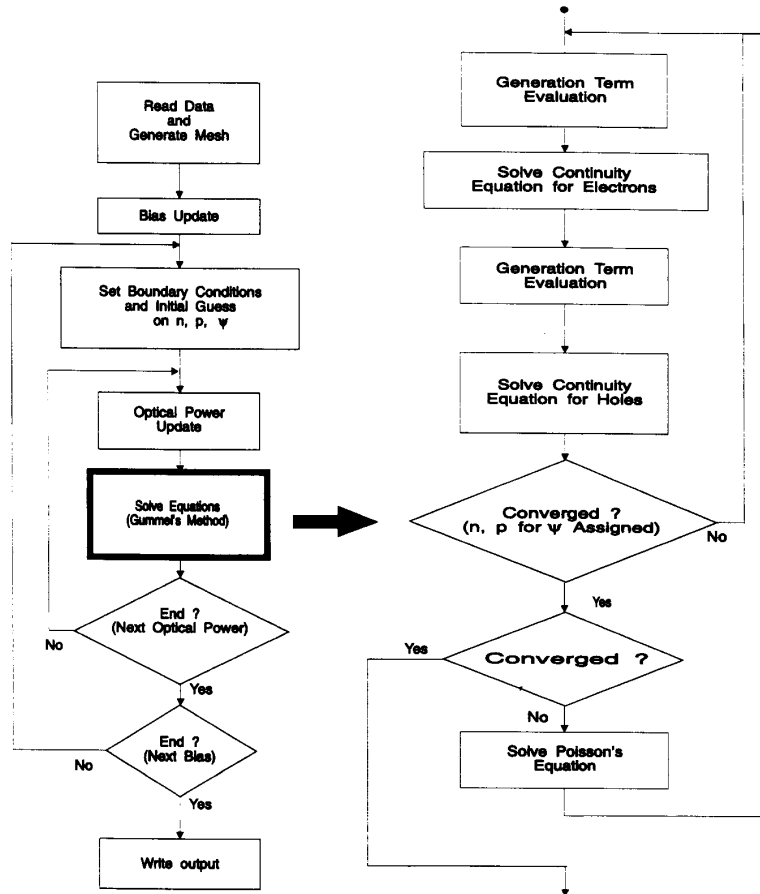


Fig. 3. Flowchart for the numerical-calculation procedure.

device. In such hypothesis both quasi-Fermi potentials for electrons and holes must coincide with the equilibrium Fermi potential  $\varphi_e$ , that is:

$$\varphi_n = \varphi_p = \varphi_e. \quad (10)$$

At the same time, for the same hypothesis of thermal equilibrium, the difference between the quasi-Fermi potentials at the border of the quasi-neutral regions, must coincide with the external applied voltage  $V$ , that is:

$$\varphi_e(0) = 0; \quad \varphi_e(x_M) = V \quad (11)$$

being 0 and  $x_M$  the device extremities in the  $x$ -direction.

The relationships of (10) and (11) represent, as a whole, the boundary conditions of the problem. The solution of the system of equations has been accomplished through the Gummel method [14].

### III. SOLUTION ALGORITHM

The flowchart for the numerical procedure is shown in Fig. 3. In the input step, the data for the device structure, including dimensions, compositions and doping concentrations as well as the material parameters are read by the program.

Then, the modulator is analysed, in a double loop, for different bias voltages and for several optical input power levels. The kernel of the solution procedure is represented by the Gummel's loop (on the right hand side of the figure), where the two continuity equations are solved iteratively with Poisson's equation. In fact, the procedure starts from an initial guess for the carrier concentrations and the potential, and it ends when the stationary condition is reached (within a fixed accuracy). A number of special algorithms have been included in the procedure in order to improve the convergence property of the solution algorithm in the case of high radiative generation, such as the introduction of an inner loop that solves only the two continuity equations for an assigned potential profile, and the gradual increase of the optical input power, which avoids the repeated calculation of the initial guess for the carrier concentrations and the potential distribution for a specified bias.

### IV. NUMERICAL RESULTS AND COMPARISON WITH EXPERIMENTS

In this section, we give an example of computed behavior for an abrupt junction (AJ) electro-absorption modulator

TABLE I  
PARAMETERS USED IN THE SIMULATION

doping n <sup>+</sup> -InP layer	$1 \times 10^{24} \text{ m}^{-3}$
doping p <sup>+</sup> -InP layer	$1 \times 10^{24} \text{ m}^{-3}$
doping absorbing layer (n <sup>-</sup> -InGaAsP)	$3 \times 10^{21} \text{ m}^{-3}$
absorbing layer depth	0.25 $\mu\text{m}$
waveguide width	1.3 $\mu\text{m}$
waveguide length	300 $\mu\text{m}$
InGaAsP static dielectric constant	13.57
InP static dielectric constant	12.40
InGaAsP high frequency dielectric constant	11.27
InP high frequency dielectric constant	9.55
conduction band discontinuity	17 eV
valence band discontinuity	32 eV

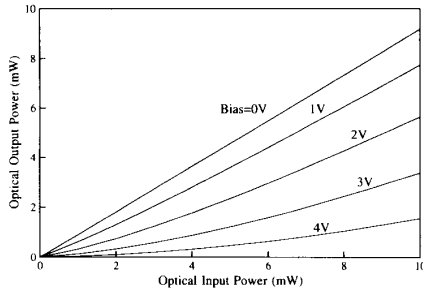


Fig. 4. Simulated AJ modulator transfer function for different applied voltages.

whose characteristics are reported in Table I.

Fig. 4 reports the transfer function of the modulator for different reverse voltages. Here, the nonlinear behavior of the device is self-evident. Note that this figure, obtained by simulation, is quite similar to the experimental results reported in [2].

To better understand the causes that generate such a bearing, it is useful to consider the electric field and the carrier distributions in the device at the front end of the device (i.e.,  $z = 0$ ). Fig. 5 shows the electric field distribution for different optical input intensities. This reveals that, as the trapped holes induce the concentration of the applied electric field at the hetero-interface, the electric field of the other region is weakened and, consequently, the total electro-absorption becomes smaller. Such a phenomenon is more accentuated as the optical intensity increases. Furthermore Fig. 5 shows that the electric field in the absorbing region is almost constant, indicating that the space-charge effect does not sensitively contribute to the degradation of the absorption properties. These results confirm that the hole pile-up, caused by the valence-band discontinuity, is the main issue in the degradation of the static performance of the device.

Fig. 6 illustrates directly the hole accumulation in the well formed at the hetero-interface. It clearly indicates that such an accumulation saturates at higher input powers. The reason for this behavior is that the hole quasi-Fermi level at high optical input power moves towards the valence band edge, and any additional carriers are then more easily transported over the barrier without being trapped in the well. The position of the hole quasi-Fermi level with respect to the valence band, for different values of the optical power, is reported in Fig. 7.

Clearly, due to the decay of the optical power along the  $z$ -direction of the device, Figs. 5–7 also represent, respectively,

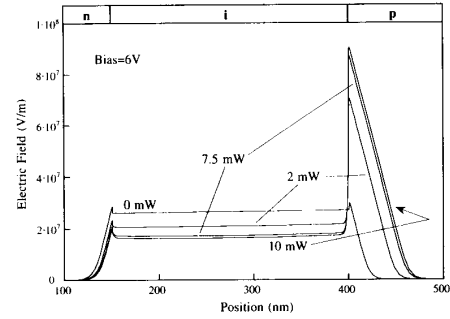


Fig. 5. Electric field distribution, in the AJ modulator, for different optical input intensities.

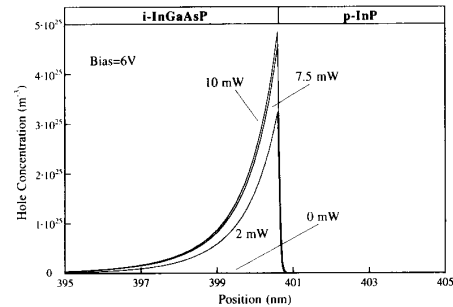


Fig. 6. Hole distribution at the hetero-interface of the AJ modulator for different optical input intensities.

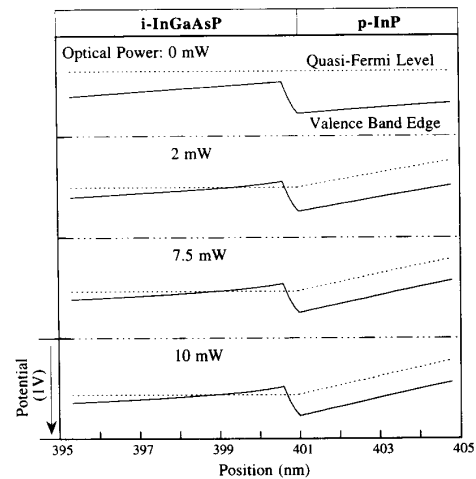


Fig. 7. Position of the hole quasi-Fermi level with respect to the valence band edge, for different optical levels at 6V bias.

the electric field, hole concentration and band structure profiles at the  $z$ -values corresponding to the different optical powers mentioned in those figures.

The hole pile-up effect is responsible for the degradation of the extinction ratio of the modulator and, consequently, affects its transmission performance. Henceforth it is important to report the optical output power versus the reverse bias voltage for different values of the input optical power.

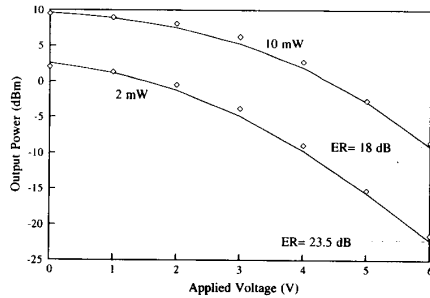


Fig. 8. Optical output power against applied voltage, for two optical intensities, for an AJ device. The continuous line indicates the simulation results. The rhombus line depicts the measured values. The extinction ratio (ER), in both the cases, has been calculated considering 0 and 6 V as the levels for space and mark, respectively.

To test our simulation model, a comparison has been made with an experimental device. This device has the same nominal structure as the one reported in [5]. The only difference is that the extinction ratio as a function of applied reverse voltage is larger in the present device, probably because, through an optimized processing procedure, the p-i junction in the present device is closer to the hetero-interface.

It is to point out that, in the simulation, the absorption coefficient (as a function of the electric field) has been determined using the experimental data at very low optical power, where the nonlinear phenomena are quite negligible. Specifically, Fig. 8 reports both the measured and the simulated optical output power versus bias voltage for two different input optical intensities. The agreement between simulation and experiment is quite good. As one could expect the extinction ratio degradation is stronger at higher input optical intensities. In particular, considering, as an example, a modulation voltage of 6 V, the extinction ratio is about 23 dB at low intensity (2 mW) and nearly 18 dB at high intensity (10 mW). These results attest that it is necessary to drastically reduce the hole-trapping effect to obtain an acceptable transmission performance.

## V. DESIGN CONSIDERATIONS FOR MODULATOR OPTIMIZATION

In this section, we deal with the design criteria for the optimization of the static characteristics of the device. It is interesting, in this contest, to consider the performance of an ideal device, that is one which is characterized by the absence of nonlinear effects (as actually occurs at very low input optical power). The calculated performance of this ideal modulator, that we call “optimum,” is used as a reference for the evaluation of realistic structures.

We have demonstrated that the valence band discontinuity at the hetero-interface p-i represents the main cause of the nonlinear behavior of the device. Two types of approach are considered here in order to strongly decrease the hole accumulation at the hetero-interface: the graded bandgap structure and the InGaAsP layer inserted structure. An earlier experimental paper has demonstrated the effectiveness of the latter approach [2]. In this contest we show how it is possible to achieve device performance close to the optimum for both approaches, explaining the reason for the success.

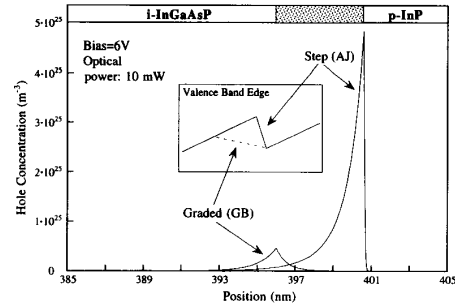


Fig. 9. Hole concentration at the hetero-interface for both step (AJ) and graded (GB) junctions. The inset shows a schematic view of the band diagram in both the cases. The shadow zone on the top indicates the transition region of the GB device.

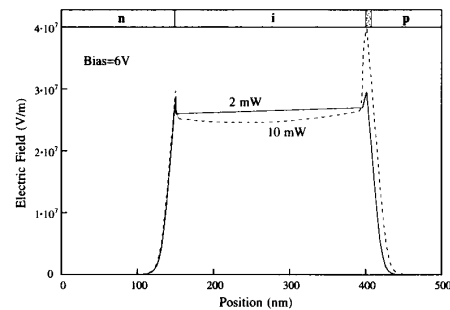


Fig. 10. Electric field distribution in the graded bandgap device, for two optical intensities. The shadow zone indicates the transition region.

### A. Graded Bandgap Layer Structure

Meaningful results have been obtained simulating a graded-bandgap structure device (GB). In this modulator the As fraction between the two materials (p-InP and i-InGaAsP) varies linearly from 0.78 to 0 over a depth of 5 nm. The substantial advantage of this structure with respect to the previous one is that it does not introduce net band discontinuities. This allows to drastically reduce the potential well height, due to the fact that the band bending due to the gap variation is compensated by that due to the electric field.

Fig. 9 shows the hole concentration in both the cases: abrupt junction and graded bandgap junction (GB) devices. It clearly depicts that, in the GB device, the hole accumulation is strongly reduced.

It is also meaningful to observe the electric field distribution in the GB device. In fact, Fig. 10 illustrates the electric field distribution in the case of gradual junction, at a fixed voltage, for two values of the optical power.

It is evident that, at least up to 10 mW of optical power, neither the hole-pile up nor the space charge effect are strong enough to degrade the modulator performance. The final result is depicted in Fig. 11, where the optical output power versus applied voltage of the GB modulator and of the AJ one are compared for two different input optical intensities. The significant result is that the saturation effect is strongly reduced in the GB device. Note that at 2 mW of optical intensity the GB device presents an extinction ratio (ER) about 4 dB higher

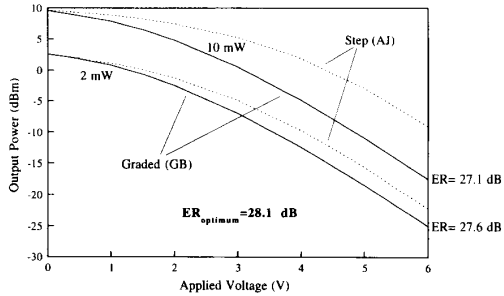


Fig. 11. Transmission performance comparison among GB (depth = 5 nm) and AJ devices. The continuous lines depict the curves obtained for the GB device. The dashed lines indicate the curves obtained for the abrupt junction device. The extinction ratio named "optimum" refers to an ideal device which does not present nonlinear effects.

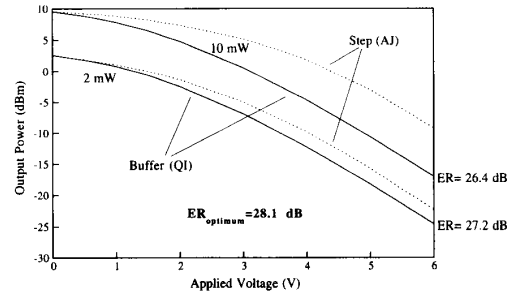


Fig. 12. Transmission performance of a QI structure with the buffer layer (depth = 5 nm) having an intermediate gap, for two values of the optical input power, compared with the AJ device.

than AJ device's, and at 10 mW such a difference increases up to 9 dB. Note also that the extinction ratio at 10 mW is degraded of only 0.5 dB with respect to that at 2 mW.

These results point out the better performance of the GB device with respect to the AJ one. Clearly, extending the graded region further would lead to even lower accumulation but, at the same time, causes a larger potential drop over the graded inactive layer at the expenses of the active one. This causes a lowering of the modulator absorption and, consequently, a weaker control capability of the modulator.

### B. The Quaternary Inserted Layer Structure

From a physical point of view, it is easy to conceive that when inserting a buffer layer of InGaAsP, whose bandgap is intermediate between those of the InP and of the InGaAsP absorbing layer, we obtain two other discontinuities in which the potential barrier is reduced of about one half; hence the accumulation of the holes decreases. Among the simulations for this type of structure the most meaningful ones are reported in Fig. 12. Here the optical output power versus the reverse modulation voltage is shown for a device with a quaternary inserted (QI) layer with an intermediate gap (depth = 5 nm) and for two values of the optical input power, compared also with the abrupt junction device. Furthermore, the curves are related with the optimum performance. It can be seen that even experiencing the QI structure it is possible to approach the optimal performance.

Actually, it would be possible to choose the As concentration for the InGaAsP buffer layer that gives the same two potential barrier heights at the two interfaces of the buffer layer. Physically this seems to be the best solution.

We have also simulated a device with a InGaAsP layer with such a As concentration, but the results obtained in this case are quite similar to those attained for the intermediate bandgap device. This can be explained considering that the hole accumulation decreases almost exponentially with barrier height, consequently even in the case of an intermediate band gap, that does not allow to divide exactly the barrier, it is possible to near the optimum performance.

We also have observed that QI layer with depth greater than 10 nm depreciate the performances due to the fact that

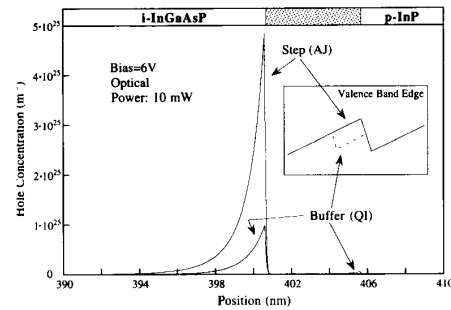


Fig. 13. Hole density distributions at 6-V bias and 10-mW optical input power, for an AJ device and an intermediate gap QI device. The inset indicates a schematic view of the band diagram in both the devices. The shadow zone indicates the quaternary inserted buffer layer. Note that the hole accumulation is strongly reduced in the QI device at both the interfaces.

the potential drop subtracted to the absorbing layer begins to be appreciable and, in a similar way to the GB structure, lower the modulation capability of the device. On the other hand in case of depths thinner than 5 nm the two wells begin to interact themselves. The hole distribution at the hetero-interfaces in the QI structure is reported in Fig. 13, also compared with that of the AJ device, considering a value of the depth of 5 nm.

## VI. DISCUSSION AND PERSPECTIVES

In the previous sections, we have demonstrated that the modulator response as a function of optical intensity is related to the hole accumulation at the hetero-interface where the valence band discontinuity occurs. We have shown that is possible to optimize the modulator performance by a suitable design of the device structure. In this section we consider some further issue in view of applications at high bit rates. We have previously shown that both QI and GB structures can be used to optimize the performance of the modulator and that they lead to quite similar performance. In the following, we will consider only the QI structure (easier to implement) to make comparison with the AJ device, since no significant advantage can be expected with the GB device with respect of the QI one.

It might be interesting to see whether the hole pile-up causes an increase of the device capacitance, an occurrence that would hindered the high-speed capabilities of the modulator. The free charge stored for unit areas in the AJ and in the QI modulators,

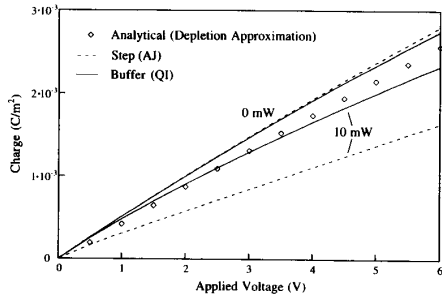


Fig. 14. Accumulated charge versus applied voltage, for both AJ and QI devices, for different values of the optical input powers. In this figure it has been arbitrary assumed that the value of the stored charge is zero at zero bias. The rhombus line shows the curve obtained by a theoretical calculation based on the depletion approximation.

as a function of applied bias at different input power levels, has been calculated directly from the simulation. The total charge stored at zero bias has been assumed to be zero for each input power. The results are shown in Fig. 14. In the case of the AJ device, one can observe that the presence of hole trapping at the hetero-interface reduces the relative variation with applied bias of the free charge stored in the device. Such effect is due to the growth of the depletion region induced by the electric field defocusing connected to the hole pile-up. In the case of the QI device the accumulated charge difference, among the curves at 0 and 10 mW, is significantly smaller than in the case of the AJ modulator.

As a whole, we can conclude that hole trapping does not, in any of the structures considered, constitute a limitation to the modulator speed.

In all cases dealt with before, we had referred to a device length of 300  $\mu\text{m}$ . However, it is important to consider shorter devices and study the influence of the length on the device performance. This is particularly significant when considering modulators for very high-speed applications (20–40 GHz), where the capacitance must be quite low. In any case a complete analysis of such situation would require a nonstationary formulation of the model, which is above the scope of this paper.

There are two main contributions to the device capacitance, coming from the depletion layer and from parasitic, respectively. The first one can be calculated approximately as [15]:

$$C = \epsilon \cdot \frac{W \cdot L}{t} \quad (12)$$

where  $W$  is the width of waveguide,  $L$  is the length of waveguide, and  $t$  is the thickness of the intrinsic layer. This means that the width and the length of the waveguide must be limited for a given application. Roughly speaking, we can say that for very high-speed applications the device length should be around 100–200  $\mu\text{m}$  [16].

Several simulations have been made for different values of the length; as a result the transmission performance versus the device length is reported in Fig. 15. Consider first the AJ modulator. It can be seen that the performance degrades as the length decreases. This occurs because the light power

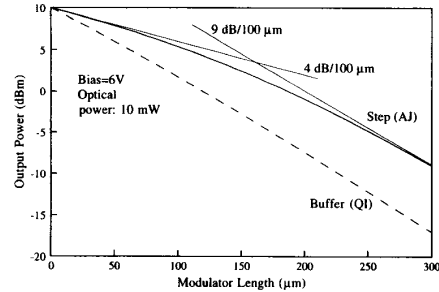


Fig. 15. Transmission performance versus device length. This is referred to both the AJ and QI devices previously considered. The applied voltage is 6 V, the optical input power is 10 mW. It is possible to notice that long AJ devices (250–300  $\mu\text{m}$ ) presents the best performances (the slope is about 9 dB/100  $\mu\text{m}$ ) while the short ones (50–100  $\mu\text{m}$ ) give the worst performances (the slope is about 4 dB/100  $\mu\text{m}$ ). On the other hand, the slope for QI device varies much less with the modulator length.

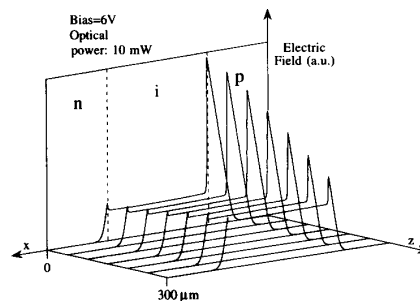


Fig. 16. Tridimensional profile of the electric field distribution in the AJ modulator (arbitrary units). Note that going towards the output of the modulator the peak of the electric field at the hetero-interface p-i decreases sensitively while the field in the absorbing region increases. This means that the nonlinear effects are stronger at the beginning of the device and lower in the direction of the end of the device.

decreases as it propagates through the device and, going towards the end facet of the device, the light intensity become small enough not to cause nonlinearity. Henceforth, if a device is sufficiently long, it can absorb an acceptable portion of the light. In other words, the impact of the nonlinearity is more remarkable in short devices. To show this fact in a more suitable fashion, Fig. 16 depicts the tridimensional distribution of the electric field along the device. On the other hand, from Fig. 15, it is possible to note that for a QI device the output power varies roughly linearly with the modulator length. This means that, as expected, this type of device is more suitable to high-speed application with respect to the AJ one.

As a result, what is reported here allows us to realize that, in the design of modulators for very-high-speed applications, the need for a strong decrease in the degradation due to nonlinearity is even more stringent, and it is necessary to enhance as much as possible the absorption characteristics of the device by an optimization of its structure.

## VII. CONCLUSION

The model reported in this paper has allowed us to evaluate in depth the static characteristics of bulk electro-absorption

modulators and to model the extinction ratio degradation. The results of the simulation agree well with experimental measurements. The simulations have revealed that the nonlinear behavior of the device is essentially due to the hole-pile up at the hetero-interface. In order to drastically reduce such an effect two possible structures have been analysed: the graded bandgap and the quaternary inserted layer structures. We have demonstrated, by several simulations, that it is possible to obtain a fairly optimized structure following both the approaches, even if the graded bandgap structure brings to the best performances. Finally, we have demonstrated that short devices for very-high-speed applications need optimization, being the saturation effects more drastic.

#### REFERENCES

- [1] F. Koyama and K. Iga, "Frequency chirping in external modulators," *J. Lightwave Technol.*, vol. 6, no. 1, pp. 87-92, 1988.
- [2] M. Suzuki, H. Tanaka, and S. Akiba, "Effect of hole pile-up at heterointerface on modulation voltage in GaInAsP electro-absorption modulators," *Electron. Lett.*, vol. 25, no. 2, pp. 88-89, 1989.
- [3] T. Kataoka, Y. Miyamoto, K. Hagimoto, K. Sato, I. Kotaka, and K. Wakita, "20 Gbit/s transmission experiments using an integrated MQW modulator/DFB laser module," *Electron. Lett.*, vol. 30, no. 11, pp. 872-873, 1994.
- [4] F. Devaux, F. Dorgeuille, A. Ougazzden, F. Huet, M. Carr, A. Carencio, M. Henry, Y. Sorel, J.-F. Kerdiles, and E. Jeanny, "20 Gbit/s operation of high-efficiency InGaAsP/InGaAsP MQW electroabsorption modulator with 1.2-V drive voltage," *IEEE Photon. Technol. Lett.*, vol. 5, no. 11, pp. 1288-1290, 1993.
- [5] P. Ojala, C. Petterson, B. Stoltz, A. C. Moerner, M. Janson, and O. Sahlén, "DFB laser monolithically integrated with an absorption modulator with low residual reflectance and small chirp," *Electron. Lett.*, vol. 29, no. 10, pp. 859-860, 1993.
- [6] M. A. Littlejohn, T. H. Glisson, and J. R. Hauser, "Hot electron transport in n-type  $\text{Ga}_{1-x}\text{In}_x\text{As}_y\text{P}_{1-y}$  alloys lattice-matched to InP," in *GaInAsP alloy Semiconductors*, T. P. Pearsall, Ed. New York: John Wiley, 1982, pp. 243-274.
- [7] T. Gonzalez Sanchez, J. E. Velazquez Perez, P. M. Gutierrez Conde, and D. Pardo Collantes, "Electron transport in InP under high electric field conditions," *Semicond. Sci. Technol.*, vol. 7, pp. 31-36, 1992.
- [8] S. Adachi, "Materials parameters of  $\text{In}_{1-x}\text{Ga}_x\text{As}_y\text{P}_{1-y}$  and related binaries," *J. Appl. Phys.*, vol. 53, no. 12, 1982.
- [9] A. G. Milnes and D. L. Feucht, "Heterojunctions and metal-semiconductor junctions," *Academic Press*, pp. 1-13, 1972.
- [10] B. E. A. Saleh and M. C. Teich, *Fundamentals of Photonics*. New York: John Wiley, 1991, pp. 248-258.
- [11] K. Tharmalingam, "Optical absorption in the presence of a uniform field," *Phys. Rev.*, vol. 130, no. 6, pp. 2204-2206, 1963.
- [12] R. H. Kingston, "Electro-absorption in InGaAsP," *Appl. Phys. Lett.*, vol. 34, no. 11, pp. 744-746, 1979.
- [13] B. R. Bennet and R. A. Soref, "Electrorefraction and electro-absorption in InP, GaAs, GaSb, InAs, and InSb," *IEEE J. Quantum Electron.*, vol. QE-23, no. 12, pp. 59-66, 1987.
- [14] H. K. Gummel, "A self-consistent iterative scheme for one-dimensional steady state transistor calculations," *IEEE Trans. Electron. Devices*, vol. ED-11, p. 455, 1964.
- [15] S. C. Lin, P. K. L. Yu, and W. S. C. Chang, "Efficient, low parasitic 1.3  $\mu\text{m}$  InGaAsP electro-absorption waveguide modulators on semi-insulating substrate," *IEEE Photon. Technol. Lett.*, vol. 1, no. 9, pp. 270-272, 1989.
- [16] G. Mak, C. Rolland, K. E. Fox, and C. Blaauw, "High speed bulk InGaAsP-InP electro-absorption modulators with bandwidth in excess of 20 GHz," *IEEE Photon. Technol. Lett.*, vol. 2, no. 10, pp. 730-733, 1990.



**D. Meglio** was born in Rome, Italy, on April 9, 1966. He received the "Laurea degree" in electrical engineering from the University of Rome "La Sapienza", Italy, in 1993.

He is currently enrolled in the doctorate program of Microelectronics and Telecommunications at the University of Rome "Tor Vergata," Italy.



**P. Lugli** graduated in Physics at the University of Modena, Italy, in 1979. In 1981, he joined Colorado State University, Fort Collins, CO, where he received the M.S. degree in 1982 and the Ph.D. degree in 1985, both in electrical engineering.

In 1985, he joined the Physics Department of the University of Modena as Research Associate. From 1988 to 1993, he was Associate Professor of Solid State Physics at the Engineering Faculty of the University of Rome "Tor Vergata". In 1993, he was appointed as Full Professor of Optoelectronics at the

same University. His current research interests involve the numerical simulation of semiconductor devices for electronics and optoelectronics applications, the Monte Carlo simulation of ultrafast phenomena in polar semiconductors, and the theoretical study of transport processes in nanostructures.

Dr. Lugli is the author of more than a hundred scientific publications, and coauthor of the book, *The Monte Carlo Modeling for Semiconductor Device Simulations*.



**R. Sabella** (M'92) was born in Rome, Italy, on December 10, 1962. He received the degree in electronics engineering (Laurea in Ingegneria Elettronica) from the University of Rome "La Sapienza" in 1987.

During 1987, he worked on the modeling of microwave devices for satellite communications. In 1988 he joined Ericsson Telecomunicazioni where he was involved in the hardware design of equipments for Telecom. Since 1989, he has been working in the research on advanced photonics technology.

He is also involved in national research programs, being responsible of a group working on the modeling of optoelectronics devices, and in a research activity on wavelength switched optical networks.

Dr. Sabella is member of IEEE/LEOS and of SPIE.



**O. Sahlén** was born in Stockholm, Sweden, in 1957. He received the M.Sc. degree in engineering physics in 1981, and the Ph.D. degree in physics in 1989, both from the Royal Institute of Technology, Stockholm, Sweden.

Between 1981 and 1984, he worked at Asea Hafa AB i Järfälla, Sweden, with development of silicon integrated electronics. Between 1984 and 1989, he worked with nonlinear optics at the Institute of Optical Research, Stockholm, Sweden. Since 1989,

he has been employed at the Fiber Optics Research Center at Ericsson Components AB, Stockholm, Sweden, where he works with integrated optics for high-speed transmission and for flexible optical networks.